Nonlinear dynamics of wind waves: multifractal phase/time effects

R. H. Mellen, I. A. Leykin

Nonlinear Processes in Geophysics (1994) 1: 51 - 56

Nonlinear Processes in Geophysics

Nonlinear dynamics of wind waves: multifractal phase/time effects

R.H. Mellen[1,2] and I.A. Leykin[1]

[1] Marine Sciences Institute, University of Connecticut, Groton CT 06340, USA
[2] Kildare Corp., 95 Trumbull St., New London CT 06320, USA

Received 15 November 1993 - Accepted 14 March 1994 - Communicated by A.R. Osborne

Abstract. In addition to the bispectral coherence method, phase/time analysis of analytic signals is another promising avenue for the investigation of phase effects in wind waves. Frequency spectra of phase fluctuations obtained from both sea and laboratory experiments follow an $F^{-\beta}$ power law over several decades, suggesting that a fractal description is appropriate. However, many similar natural phenomena have been shown to be multifractal. Universal multifractals are quantified by two additional parameters: the Lévy index $0 \leq \alpha \leq 2$ for the type of multifractal and the co-dimension $0 \leq C_1 \leq 1$ for intermittence. The three parameters are a full statistical measure the nonlinear dynamics. Analysis of laboratory flume data is reported here and the results indicate that the phase fluctuations are 'hard multifractal' ($\alpha > 1$). The actual estimate is close to the limiting value $\alpha = 2$, which is consistent with Kolmogorov's lognormal model for turbulent fluctuations. Implications for radar and sonar backscattering from the sea surface are briefly considered.

1 Introduction

Analysis of radar and sonar backscattering from the sea surface requires a model of the wave dynamics (Bass and Fuchs, 1979). Linear theory is often used and suffers from neglect of important nonlinear features of wind waves. Two of these are wavefront steepening and instability.

Wavefront steepness means that harmonics tend to be locked together so that their average phase speeds are the same. Doppler shifts in high-frequency backscatter experiments should therefore not be expected to follow linear dispersion theory (Mellen, 1991). Also, skewness of the waveforms causes an up/downwind asymmetry in backscatter strength (Chen and Fung, 1990).

Instability is the basic mechanism for wave growth (Phillips, 1966) and also appears to be responsible for the breakup into sporadic wave-groups. It should not be too surprising if the associated phase fluctuations turn out to be fractal. Bragg-scatter theory is based on a random-phase approximation and fractal statistics can be quite different.

Wave groups observed in flume and ocean experiments appear to be similar. Huang (1991) examined wave-buoy data by phase/time analysis of the analytic signal and found evidence of groups. He also found that the frequency spectrum of the phase fluctuations follows an $F^{-\beta}$ power law over several decades and the lack of a characteristic scale suggested a simple fractal description involving a single dimension. Laboratory measurements reported here support Huang's results in some detail and this agreement gives hope that our extended results may also be representative of the open ocean.

Simple scaling implies linearity. Natural phenomena are generally nonlinear and also multifractal; i.e., they have a spectrum of dimensions and not simply one. It is the generic '1/F noise' problem, wherein incoming low-frequency energy is pumped up to ever higher frequencies and ultimately dissipated, yielding an equilibrium $F^{-\beta}$ spectrum in the mid-range. Sporadic properties or intermittence show up as a high upper tail in the probability density (PD).

For 'universal' multifractals, the scaling is quantified by two additional parameters: the Lévy index $0 \leq \alpha \leq 2$ for the type of multifractal and the co-dimension $0 \leq C_1 \leq 1$ for the intermittence (Schertzer and Lovejoy, 1988). The three parameters are then a full statistical measure of the nonlinear cascade and details of the underlying dynamics need not be considered. The results presented here indicate that the phase fluctuations of wind-generated waves are also multifractal.

2 Flume experiment

Figure 1 shows a sketch of the wave flume and the experimental configuration. The length and depth of the flume are approximately 4 m and 40 cm, respectively, and the water depth 30 cm. The wave height measurements were made at fetch of about 3 m and wind speed of about 7 m/s.

Correspondence to: R.H. Mellen

Vertical displacement vs. time was measured by means of a simple conductance wavegauge. Signal voltage was recorded digitally at 128/sec for a total period of 64 sec. and the data filed for later analysis.

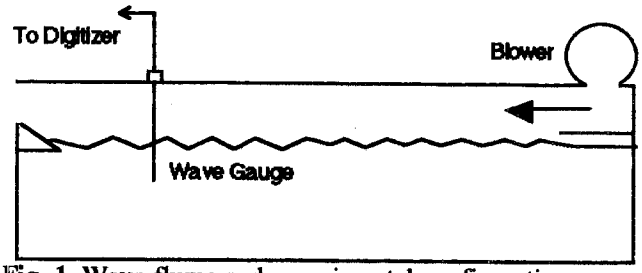

Fig. 1. Wave flume and experimental configuration.

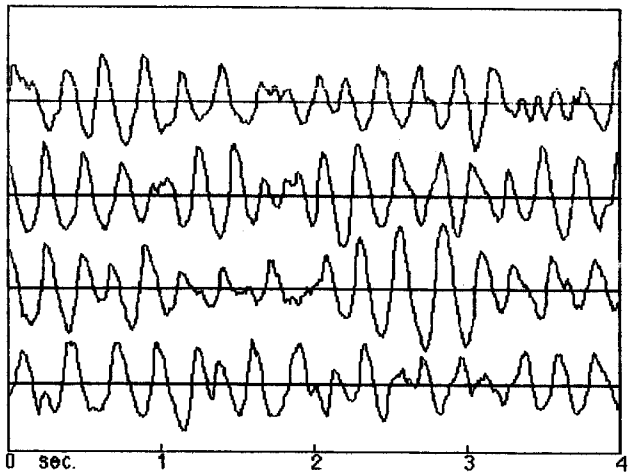

Fig. 2. Portion of the record of waveheight $\zeta(t)$.

A portion of a wave record is shown in Fig. 2. The rms waveheight is roughly 3 mm and maximum peak-to-trough amplitude is roughly 1 cm. The waveforms clearly show steepening of the wavefronts, particularly for the higher amplitudes. There is also evidence of sporadic groups that consist of only a few cycles and highly irregular behavior between groups.

3 Spectrum analysis

Frequency spectra were obtained by fast fourier transform (FFT) at 256 points per sample using a Hanning window and averaging over 60 samples. The maximum usable frequency F_{max} is taken as 50 Hz.

The power spectrum in Fig. 3 has a center frequency near 4 Hz and a rather narrow bandwidth. The small bump at 8 Hz is the only evidence of harmonics associated with the steep wavefronts.

The bispectrum is also useful for examining nonlinear phenomena in wind waves (Hasselmann et al., 1963). The bispectrum is a measure of third moments, which involves sum and difference frequencies. However, the relations are given simply by the product of Fourier coefficients of the frequencies F_1, F_2 times coefficients of the sum frequency F_1+F_2.

Bispectral coherence is better suited for examining the phase relations between harmonics and is obtained simply normalizing the bispectrum.

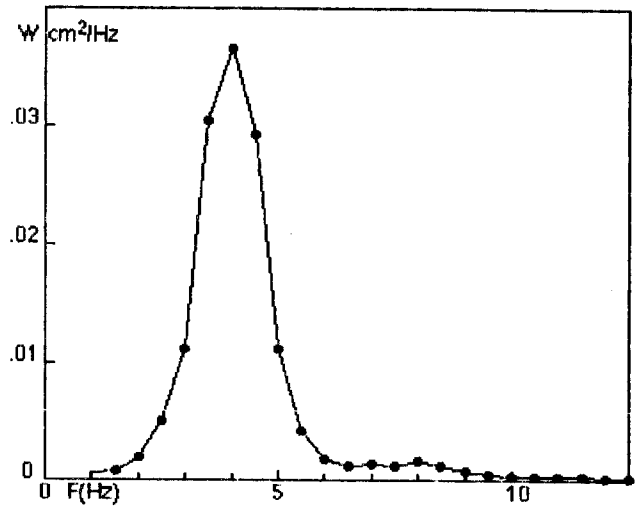

Fig. 3. Frequency spectrum of the wave record.

The bicoherence formula used here is:

$$P+iQ = \frac{\langle S(F_1)S(F_2)S^*(F_1+F_2)\rangle}{\langle |S(F_1)S(F_2)S^*(F_1+F_2)| \rangle}, \qquad (1)$$

where S(F) is a complex Fourier coefficient, S*(F) is the conjugate, bars indicate absolute values and the brackets indicate expectations. Bicoherence is real for waves that are spatially symmetric to time reversal and imaginary for antisymmetric

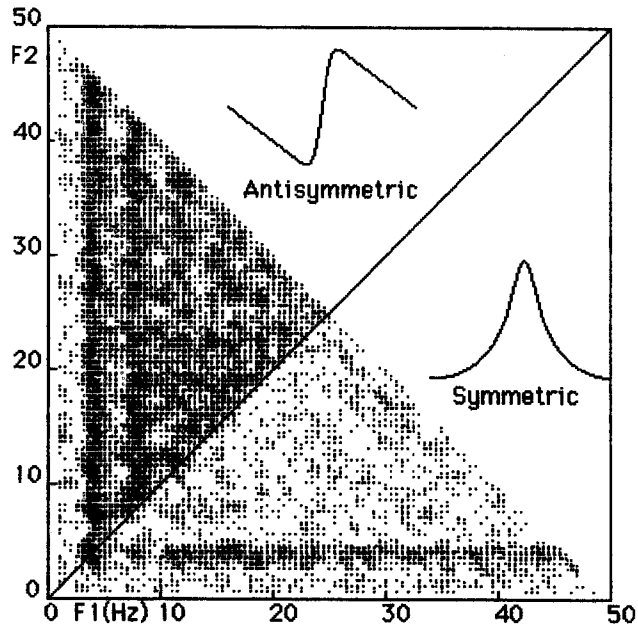

Fig. 4. Bicoherence spectrum of the wave record, showing the symmetric and antisymmetric components.

Since F_1 and F_2 are interchangeable and $F_1+F_2 \leq F_{max}$, all the non-redundant values of P and Q are contained in triangles with baseline on either frequency axis.

The 2-D bicoherence frequency-spectrum of the wave data is shown in Fig. 4. The gray scale corresponds to 9 linear steps covering the range 0 to 0.5. Spatial skewness clearly dominates and harmonic coherence is rather high, both of which are consistent with steep wavefronts. Fluctuations are evident in the frequency spreads and this suggests an underlying stochastic modulation process.

4 Analytic signal

While the Fourier methods measure only time-average properties of a signal, the analytic-signal method is useful for examining 'instantaneous' behavior in terms of envelope and phase. The analytic signal is given by:

$$Z(t)=\zeta(t)+i\xi(t)\,, \qquad (2)$$

where $\zeta(t)$ is a real signal and $\xi(t)$ is its Hilbert transform, which is obtained here by the usual FFT/invFFT method. The phase $\emptyset(t)$ and envelope E(t) are given by:

$$\emptyset(t)=\arctan[\xi(t)/\zeta(t)],\quad E(t)=[\zeta(t)^2+\xi(t)^2]^{1/2}. \qquad (3)$$

Then $\emptyset(t)$ is approximated as:

$$\emptyset(t)=\omega_0 t+\delta\emptyset(t)\,, \qquad (4)$$

where ω_0 is the mean angular frequency and $\delta\emptyset(t)$ is phase deviation.

In most of the early work, $\emptyset(t)$ was confined to the range $0 \leq \emptyset \leq 2\pi$ (Melville, 1983). Huang 'unwrapped' his data and detrended to remove the $\omega_0 t$ term. The frequency spectrum of the phase fluctuations showed no characteristic scale and this suggested a fractal description.

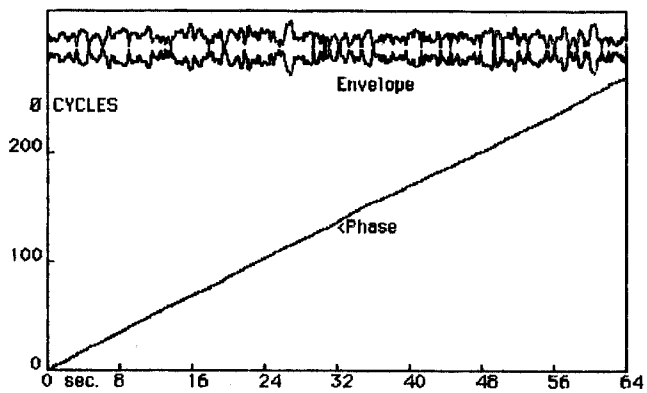

Fig. 5. Phase and envelope by the phase/time method.

Plots of phase and envelope of the flume data are shown in Fig.5. For clarity, the envelope was smoothed slightly by low-pass filtering to better illustrate the sporadic nature of group structure.

Figure 6 are the phase fluctuations obtained by detrending the phase in Fig. 5. 'Unwrapping' is potentially ambiguous for noise-like signals; however, two different algorithms were used and there were no significant changes in the results.

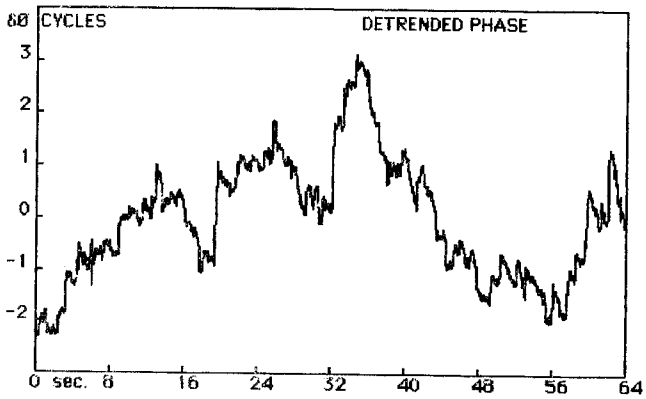

Fig. 6. Detrended phase fluctuations.

5 Fractal analysis

For frequency spectra following an $F^{-\beta}$ power law, the simple fractal dimension is given by $D=(5-\beta)/2$ (Berry and Lewis, 1990).

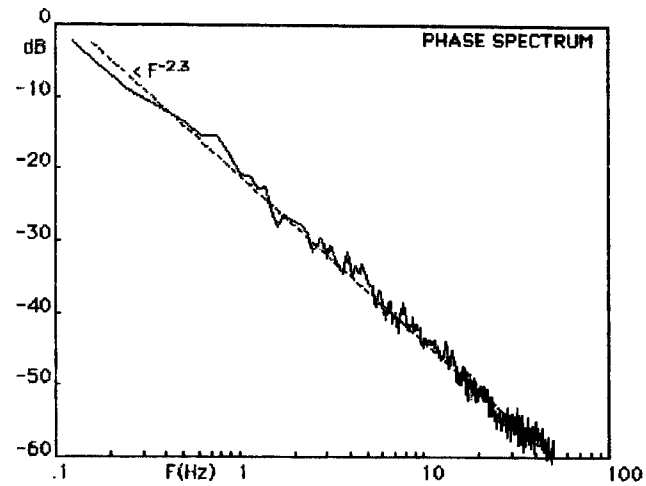

Fig. 7. Frequency spectrum of phase fluctuations.

The frequency spectrum of the phase fluctuations $\delta\emptyset(t)$ is shown in Fig. 7. Note there is no apparent characteristic scale in this frequency range. The dashed line is the fit with $\beta=2.3$ and therefore $D\approx1.35$. Huang's value was $\beta\approx2.2$, for which $D\approx1.4$.

Alternative methods of calculating a fractal dimension are the 'coastline' and 'box count' methods (Feder, 1988). The first measures chord length of the data set vs. resolution. The second counts the number of data points falling within boxes as a function of box size. The sampling intervals are taken here as $\tau=T/2^m$, where $m=1,2,\cdots$, T is the total time of the data set and n(m) is the result of the respective calculations.

The respective analyses of the phase data are shown in Fig. 8. The slopes k of $M=\log_2[n(m)]$ vs. m are obtained

by linear regression (dashed lines). The fractal dimensions are D=1+k for the 'coastline' method and D=k for the 'box count' method; therefore, D≈1.34 for both cases.

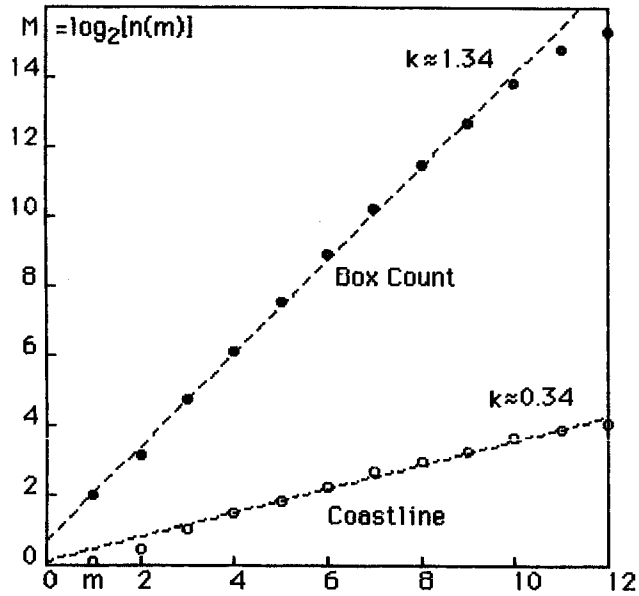

Fig. 8. Fractal analysis of the phase fluctuations.

6 Multifractal analysis

For simple scaling, the moments have specific relations analogous to a gaussian distribution. Systematic deviation from these relations reflect the sporadic properties or 'intermittence' of a multifractal process. The analysis method of Lardner et al. (1992) is used here because of its relative simplicity.

The theory treats the series A(t) as a random walk (RW), where β/2 is fractional order of integration (Feder, 1988). In general, the qth moments of increments vs. resolution should scale as:

$$\langle |\Delta A_\tau|^q \rangle = \langle |A(t)-A(t+\tau)|^q \rangle \propto \tau^{k(q)}, \qquad (5)$$

where q is any moment, including non-integral values.

Figure 9 illustrates the method, where τ=N/n, N is the total number of data points in the set and sampled points in the example are indicated by the solid circles. As before, τ is decreased sequentially by factors of two.

Some insight into the method is gained by considering the second moment of Eq. 5. For a frequency spectrum $|S(F)|^2 \propto F^{-\beta}$ in the range $F_1 \le F \le F_2$:

$$\langle |\Delta A_\tau|^2 \rangle \propto \int_{F_1}^{F_2} dF\, F^{-\beta} [1-\cos(2\pi F\tau)] \propto \tau^{\beta-1} \propto \nu^{1-\beta}. \qquad (6)$$

Then β≈1+k(2), where k(2) is measured in a corresponding range of ν. The accuracy of approximation depends on both β and bandwidth.

The multifractal measure is K(q) where:

$$K(q)=qk(1)-k(q)=\frac{C_1(q^\alpha-q)}{\alpha-1}. \qquad (7)$$

The limiting multifractal types are monofractal (α=0) and lognormal (α=2).

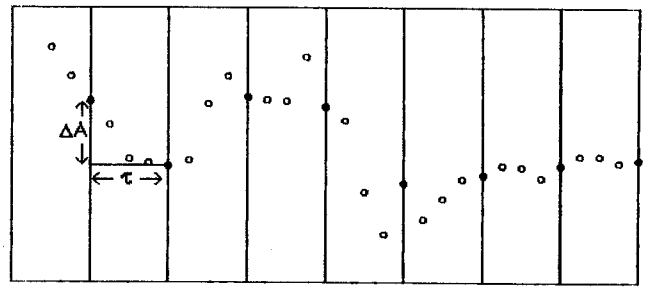

Fig. 9. Example of the multifractal sampling procedure.

In the present case, A(t)=δØ(t). Analysis in terms of the sampling frequency ν is preferred in order to show results as frequency spectra. The moment values are summed over the data set and averaged as follows:

$$n(m)=(1/\nu)\sum_{\mu=1}^{\nu} |\Delta A_{\nu\mu}|^q, \quad \nu=2^m. \qquad (8)$$

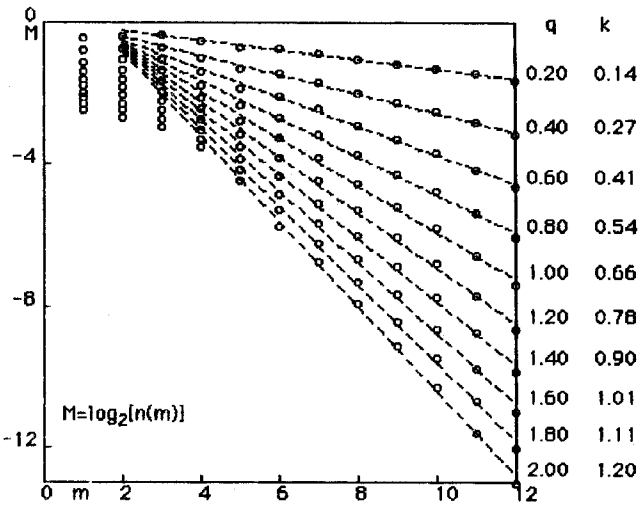

Fig. 10. Multifractal moment analysis.

Plots of M vs. m for the δØ data are shown in Fig. 10. Deviation from linearity in the lower range apparently reflects an outer scale, which is not seen in the spectra of Fig. 7 because only about 8 octaves were covered. Only the 7 highest points were used in the regressions in Fig. 10.

The dashed lines are the regression fits and k(q) estimates for the selected q's are shown at the right. The estimated value β≈1+k(2)≈2.2, which is slightly lower than the FFT estimate β≈2.3.

Estimation of parameters α and C_1 is shown in Fig. 11. The solid circles are the phase data and the dashed curve is the formula fit with α=2, C_1=0.06.

According to theory, $\alpha=2$ is consistent with a lognormal PD of the increments. Since $C_1<<1$, the process is quite homogeneous; i.e., not highly intermittent.

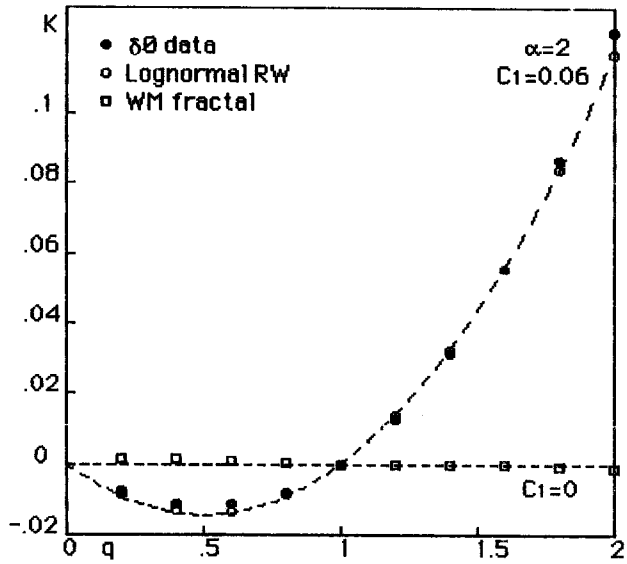

Fig. 11. Multifractal parameter analyses.

For the special case $\beta=2$, the RW becomes equivalent to a summation of independent impulses whose strength statistics depend on the type of process. For comparison purposes, a lognormal RW realization was generated using a gaussian number-generator with variance $\sigma^2=1$ and then exponentiating and summing the increments with random signs. Since $\beta=0$ for the increments, $\beta=2$ for the RW. The open circles in Fig. 11 are the results of the analysis. Note that $C_1\approx0.06$ here also, which is evidently fortuitous.

The squares in Fig. 11 represent results of analysis of a Weierstrass-Mandelbrot fractal generated with D=1.5, which effectively gives $\beta=2$ (Berry and Lewis, 1980). For simple-scaling, $C_1=0$ and agreement with theory is good

7 Probability density

Figure 12 compares logarithmic PD's of the phase data (solid circles) with the lognormal RW case (open circles). The abscissa is $\ln|\Delta|$, where the $|\Delta|$'s are finite differences (absolute values) measured at the highest resolution. Since the data sets were adjusted in amplitude to set the peaks close to zero, the scale is arbitrary. The solid curve is the lognormal case with unit variance.

The main problem with the phase PD is the high lower tail. To examine this, the lognormal RW case is further analyzed via the PD vs. step-size.

The sampling increments for a RW are:

$$\Delta_n=\sum_{i=1}^{n}\Delta_i\ , \qquad (9)$$

where n is the number of steps in the samples. In Fig. 9, n=4. Moment expectations then scale as $n^{k(q)}$, where k(q) depends on the PD of Δ. The method of calculation PD vs. n is outlined in Appendix A. Since no solution is known for n>1, the PD's were calculated numerically.

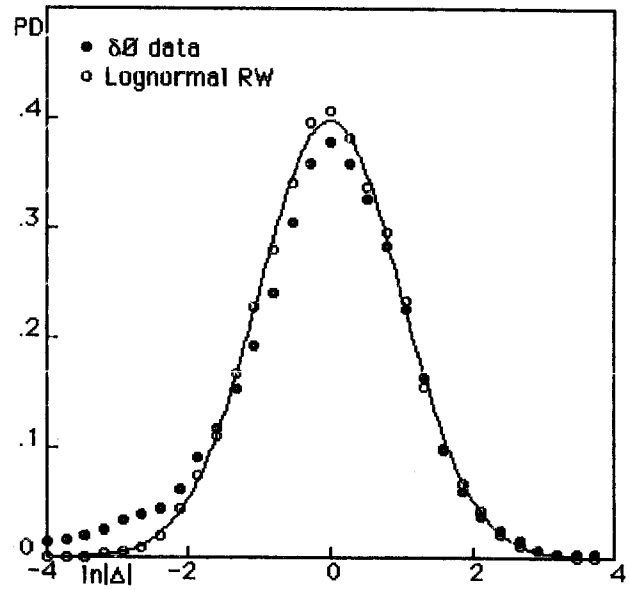

Fig. 12. Logarithmic probability density plots.

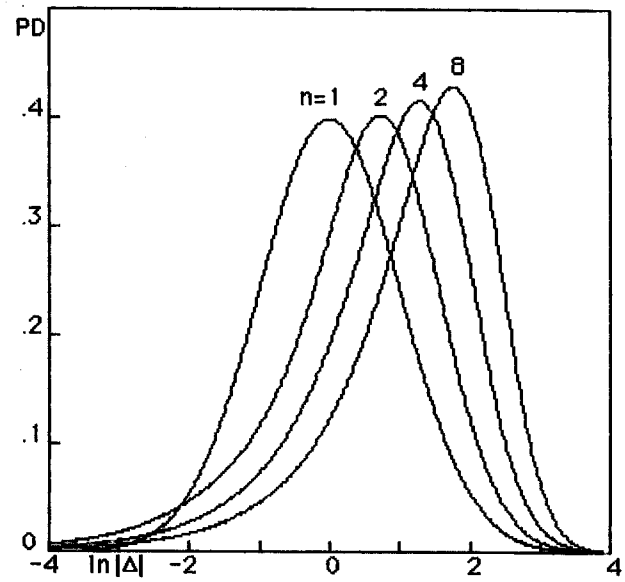

Fig. 13.Lognormal PD vs. step size n.

Figure 13 shows the logarithmic PD's for unit variance calculated numerically by the PD method vs. step size n.

A similar plot for the phase can also be obtained by direct sampling of the data set. Figure 14 shows the logarithmic PD of the phase data for the same n range as in Fig. 13. The solid curve is lognormal with unit variance. While the trends are similar, the n=1 case is more consistent with the n=2 case in Fig. 13, which suggests that the logarithmic

'singularities' are not fully developed or the measurement resolution is too low to see them.

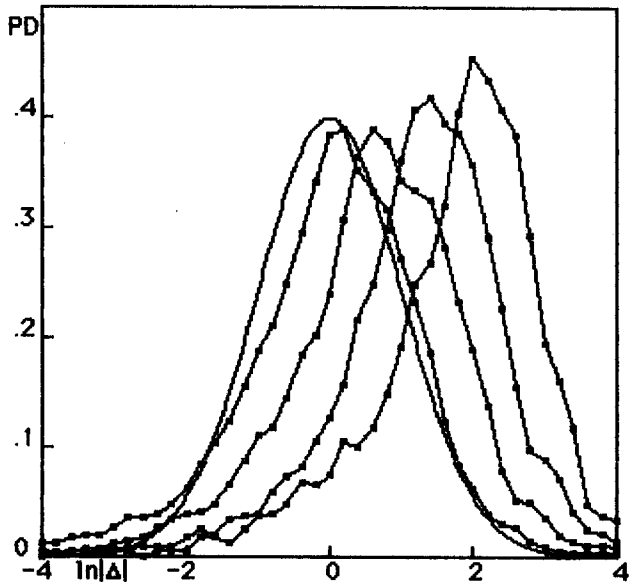

Fig. 14. Log PD of δØ data vs. step size n.

8 Conclusion

Lévy index $\alpha>1$ is classed as 'hard multifractal' and the limiting value $\alpha=2$ is lognormal. The present results indicate that the phase fluctuations of wind waves are, to good approximation, lognormal. Significance of these results to the backscattering problem probably lies mainly in the fluctuation statistics, which can be expected to have more extreme variability than the conventional gaussian model predicts.

It is interesting to note that recent investigations of Kolmogorov's model (Kolmogorov, 1962) gave rise to 'universal' multifractal theory. Lognormal statistics are common to a broad range of phenomena in many different disciplines (Aitchison and Brown, 1957) and therefore might well be expected to apply to the present case as well as to other kinds of similar fluctuations.

Appendix A

Consider a normal RW where the PD of increments Δ is:

$$p(\Delta)=\frac{\exp(-\Delta^2/2\sigma^2)}{(2\pi\sigma^2)^{1/2}}=P(\Delta_1),\ n=1. \tag{1A}$$

The joint PD is integrated iteratively as follows:

$$P(\Delta_{n+1})=\int_{-\infty}^{\infty}d\Delta_n\, P(\Delta_n)p(\Delta_{n+1}-\Delta_n), \tag{2A}$$

and the simple result is:

$$P(\Delta_n)=\frac{\exp(-\Delta^2/2n\sigma^2)}{(2\pi n\sigma^2)^{1/2}}. \tag{3A}$$

For the lognormal RW, the PD of increments Δ is:

$$p(\Delta)=\frac{\exp[-(\ln|\Delta|)^2/2\sigma^2]}{|\Delta|(8\pi\sigma^2)^{1/2}},\quad -\infty<\Delta<\infty. \tag{4A}$$

It is useful to transform to the variable $x=\ln|\Delta|$. Then:

$$P(x_1)=\frac{\exp(-x_1^2/2\sigma^2)}{(2\pi\sigma^2)^{1/2}},$$

$$P(x_{n+1})=\int_{-\infty}^{\infty}dx_n P(x_n)\times$$

$$\left\{\frac{\exp[-(\ln u)^2/2\sigma^2]}{u}+\frac{\exp[-(\ln v)^2/2\sigma^2]}{v}\right\}, \tag{5A}$$

where $u=|\exp(x_n)-\exp(x_{n+1})|$, $v=\exp(x_n)+\exp(x_{n+1})$.

References

Aitchison, J. and Brown, J. A., *The Lognormal Distribution*, Cambridge University Press, Cambridge, 1957.

Bass, F. G. and Fuks,I. M., *Wave Scattering From Statistically Rough Surfaces*, Pergamon, New York, 1979.

Berry, M. V. and Lewis, Z. V., On the Weierstrass-Mandelbrot fractal function, *Proc. R. Soc. Lond. A 370*, 459-484, 1980.

Chen K. S. and Fung, A. K., A Bragg scattering model for skewed sea surface, *IEEE Oceans '90 Proceedings*, 249-252, 1990.

Feder, J., *Fractals*, Plenum Press, New York, 1988.

Hasselmann, K., Munk, W., and MacDonald, G., Bispectra of ocean waves, in *Time Series Analysis*, pp. 126-139, ed. Rosenblatt, M., J. Wiley & Sons, New York, 1963.

Huang, N. E., The local properties of ocean surface waves by the phase-time method, *Nonlinear Water Waves Workshop Proceedings*, Bristol, U. K., 1991.

Kolmogorov, A. N., A refinement of previous hypothesis concerning the local structure of turbulence in a viscous incompressible fluid at high Reynolds number, *J. Fluid Mech. 13*, 82-85, 1962.

Lardner, C. S., Desaulniers-Soucy, N., Lovejoy, S., Schertzer, D., Braun, C. and Lavallée, D., Universal multifractal characterization and simulation of speech, *Int. J. Bifurcation and Chaos, 2*, 715-719, 1992.

Mellen, R. H., Nonlinear effects in wind-wave generation, in *Ocean Variability and Acoustic Propagation*, pp 187-198, eds. Potter, J. and Warn-Varnas, A., Kluwer Academic, Dordrecht, 1991.

Melville, W. K., Wave modulation and breakdown, *J. Fluid Mech., 128*, 489-506, 1983.

Phillips, O. M., *The Dynamics of the Upper Ocean*, Cambridge University Press, Cambridge, 1966.

Schertzer, D. and Lovejoy, S., Nonlinear variability in geophysics: multifractal simulations and analysis, in *Fractals' Physical Origin and Properties*, pp. 49-79, ed. Pietronero, L., Plenum, New York, 1988.